

Article

# Renewable Energy Potential by the Application of a Building Integrated Photovoltaic and Wind Turbine System in Global Urban Areas

Jaewook Lee <sup>1</sup>, Jeongsu Park <sup>2</sup>, Hyung-Jo Jung <sup>2,\*</sup> and Jiyoung Park <sup>3,\*</sup> 

<sup>1</sup> Illinois School of Architecture, University of Illinois at Urbana-Champaign, Champaign, IL 61820, USA; jlee764@illinois.edu

<sup>2</sup> Department of Civil and Environmental Engineering, KAIST, Daejeon 305-701, Korea; hjung@kaist.ac.kr

<sup>3</sup> Department of Architecture, Inha University, Inharo 100, Nam-gu, Incheon 402-751, Korea

\* Correspondence: hjung@kaist.ac.kr (H.-J.J.); jypark@inha.ac.kr (J.P.);  
Tel.: +82-42-350-3626 (H.-J.J.); +82-32-860-7583 (J.P.)

Received: 25 November 2017; Accepted: 13 December 2017; Published: 17 December 2017

**Abstract:** Globally, maintaining equilibrium between energy supply and demand is critical in urban areas facing increasing energy consumption and high-speed economic development. As an alternative, the large-scale application of renewable energy, such as solar and wind power, might be a long-term solution in an urban context. This study assessed the overall utilization potential of a building-integrated photovoltaic and wind turbine (BIPvWt) system, which can be applied to a building skin in global urban areas. The first step of this study was to reorganize the large volume of global annual climate data. The data were analyzed by computational fluid dynamic analysis and an energy simulation applicable to the BIPvWt system, which can generate a  $P_{\max}$  300 Wp/module with a 15% conversion efficiency from a photovoltaic (PV) system and a 0.149 power coefficient/module from wind turbines in categorized urban contexts and office buildings in specific cities; it was constructed to evaluate and optimize the ratio that can cover the current energy consumption. A diagram of the distribution of the solar and wind energy potential and design guidelines for a building skin were developed. The perspective of balancing the increasing energy consumption using renewable energy in urban areas can be visualized positively in the near future.

**Keywords:** building integrated skin system; renewable energy potential; energy simulation; design guideline; computational fluid dynamic analysis

## 1. Introduction

The need and flow of energy in urban areas has increased rapidly. Currently, approximately 3.2 billion people live in urban areas and the urban population is expected to increase to approximately 5 billion by 2030 [1]. Among those cities, most areas show large and small issues related to environmental and energy problems [2]. Buildings are responsible for 30–40% of all primary energy and 40–50% of greenhouse gas emitted [3]. Therefore, the increasing energy concerns to maintain the balance between energy supply and demand are being managed using several methods: optimization of energy consumption, design guidelines and strategies, and application of renewable energy.

Energy use in the building sector can be optimized using a range of technological developments and skills. The energy used in buildings is composed mainly of heating, cooling, and lighting. In regions where heating is dominant, especially in northern Europe, the proportion accounts for approximately 70% of the total energy, and in regions where cooling is dominant, the cooling load accounts for more than 70% of the total [4–6]. Of course, lighting comprises a considerable portion of the office building, which ranges from approximately 15% to 50%. These values may vary in proportion

or absolute value according to changes in the input parameters, such as the building type, orientation, and heating, ventilation, and air-conditioning (HVAC) schedule [7]. Several optimization simulation programs and theories, such as a genetic algorithm, have been applied to urban areas and buildings through optimization [8–12]. As a maintenance phase, advanced control system methods have been introduced for energy and occupant comfort [13]. In addition to the building form and control technique, optimization of the components of a building skin have been introduced, which also works effectively as energy management [14–17].

Second, the approach by presenting strategies, such as design guideline work, effectively improves the building aesthetics and reduces the energy consumption in buildings and urban areas [18]. Some related studies examined how urban and building design can work effectively under certain climate conditions. Therefore, thermal comfort analysis was performed in certain climates and the strategy-related form, orientation, and spatial layout essential to the proper performance were handled [19–21]. As another guideline, solar and lighting design technologies were evaluated in terms of their effects on energy, environment, and health [22–24].

In addition, although architects and engineers can reduce their energy consumption through optimization and design, buildings and urban areas are some of the main sources of energy expenditure, which inevitably require the application of renewable energy for urban sustainability. As the main applicable source in building and urban areas, researchers have mainly examined photovoltaics (PV), wind, bio, and geothermal energy [25,26]. The economic value and financial analysis of those energy sources was performed and their technological competitiveness is increasing [27]. In addition, studies related to building-integrated renewable energy systems, such as PV thermal systems and window-integrated transparent PV systems, have been performed [28,29]. As an application of renewable energy, studies involving solar radiation analysis, the PV tracking system, and increasing wind turbine performance have been conducted [30–32], and the visual impact of building integrated photovoltaics (BIPV) [33] and the application of BIPV on a wall system [34] have been investigated. In addition, as a hybrid system, the prospect of an integrated PV and wind turbine system was studied [35–37]. Several studies have examined a range of solar and wind power systems, e.g., sun tracking PV and wind hybrid systems [38], the optimal size of the PV and wind hybrid system [39], and the validity of PV and wind energy harvesting in double skins [40–42]. Hence, the main topic of the current study was to increase the efficiency of PV or wind power, improve their applicability and feasibility, or apply large-scale hybrid systems. Accordingly, it is necessary to develop and analyze a hybrid system that is applicable on a small scale, particularly a building facade.

In this paper, the solar and wind energy potential in urban areas was estimated by applying buildings with an integrated PV and wind turbine (BIPvWt) system. The proposed BIPvWt system has an advantage in attaching to a building skin to generate sustainable and clean energy, and it was initially introduced as a building-integrated wind turbine (BIWt) system [43]. The integration of a micro wind turbine with the ventilated building skin for energy harvesting was a fairly new design concept. Based on the basic principle of this system, a more sophisticated device was tested and an evaluation of the renewable energy potential of a building system in global urban areas could be implemented. In addition, the BIPvWt system was introduced and the performance of the energy generation potential in different cities was evaluated as an application of the system to the building area. Eventually, a feasibility study will be performed by simulating and optimizing the application of a BIPvWt system in the perspective of both design and engineering as a contribution towards balancing energy consumption and generation in urban areas.

## 2. Methods

This section presents the methodology used in this study to determine the renewable energy potential and energy consumption and generation in a specific region. For the input data, several variations, such as climate and the PV and wind turbine properties, were tested.

The analysis procedure was as follows:

- Introduce a proposed BIPvWt system
- Classify the climate data in global cities
- Plot an energy potential chart and diagram by the variation of solar irradiation and wind power
- Set the building module and BIPvWt system for energy generation and consumption output
- Analyze the energy balance as an application of the BIPvWt in specific areas in terms of energy consumption and generation.

### 2.1. Climate Data

The climate data was selected from the American Society of Heating, Refrigerating, and Air-Conditioning Engineers (ASHRAE) and Energy Efficiency & Renewable Energy (EERE), which have information on more than 2100 city locations [44]. The paper selects 143 representative cities as variables to compare the solar and wind energy potential in the ASHRAE climate data. They are the major cities in Europe and Asia, and in each state of the U.S. Some cities are capitals of each country or state, and the others are selected based on the population and population density. In addition, the U.S. has the most cases compared to other areas because the climate data is well distributed in terms of climate classification and the weather data is relatively convincing. Each zone was classified according to the ASHRAE standard, which ranges from zone 1 (very hot) to 8 (subarctic), and the zone was analyzed using the thermal and humidity criteria. The population and density data in selected cities were well defined and informed (Demographia 2015). Figure 1 presents a histogram of the city lists according to the ASHRAE climate classification.

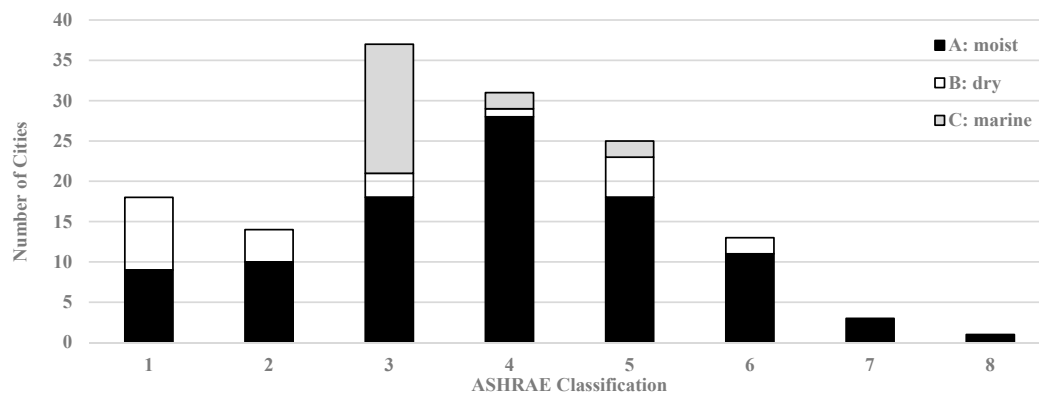


**Figure 1.** Histogram of 143 cities according to the American Society of Heating, Refrigerating, and Air-Conditioning Engineers (ASHRAE) classification.

### 2.2. Energy Simulation and Input Data

Two simulation programs were used to evaluate the energy potential, BIPvWt: the ESP-r simulation program for an analysis of the PV and building energy consumption, and ANSYS Fluent for a computational fluid dynamics (CFD) analysis of the performance of the wind power conversion system [8,45]. ANSYS Fluent is one of the most-used CFD software offering various turbulence models based on the Reynolds-Averaged Navier Stokes (RANS) model. The power production of the wind turbines is estimated by an examination of the wind speed distribution around the applied system through CFD analyses. The ESP-r software package is recognized and used widely in more than 70 countries as an industry standard for the simulations. The authors employed ESP-r 11.1, which considers the energy use of heating, cooling, lighting, and PV energy generation. Thus, ESP-r has been used extensively to assess building energy applications, particularly as a simulation tool to compare various cities [14,29]. In addition, the energy performance of the PV module has been analyzed based on information, such as the open circuit voltage ( $V_{oc}$ ), short circuit current ( $I_{sc}$ ), and maximum power point voltage ( $V_{mpp}$ ) in the simulation [46]. The information on the solar PV

for the energy simulation is based on the data provided by the manufacturer for a silicon-based PV system [47].

As the input variables, three types of building facade including BIPvWt system and climate change in each city were applied. As the output variables, building energy consumption (heating, cooling, and lighting energy) and generation (PV and wind turbine) were considered. As simulation modeling, the office building was comprised of 4 perimeter zones, 4.57 m (15 ft) in depth and 6.10 m (20 ft) in width, with a floor-to-floor height of 3.05 m (10 ft) [13,48], as shown in Figure 2A. Three different simulation cases were considered: (1) 100% Window Wall Ratio (WWR)—“b1” Basic module; (2) 33% WWR—“b2” Basic module 2; and (3) 33% WWR with BIPvWt system—“BI”, as shown in Figure 2B–D, respectively. The  $U$ -factor of the envelopes was set by the ASHRAE standard, 100% WWR was used as the basic module, and 33% WWR was used as the BIPvWt building type. The height of the building used in the simulation was set as the highest skyscraper in this study, which can avoid the local factor of wind disturbance and inference on an urban scale.

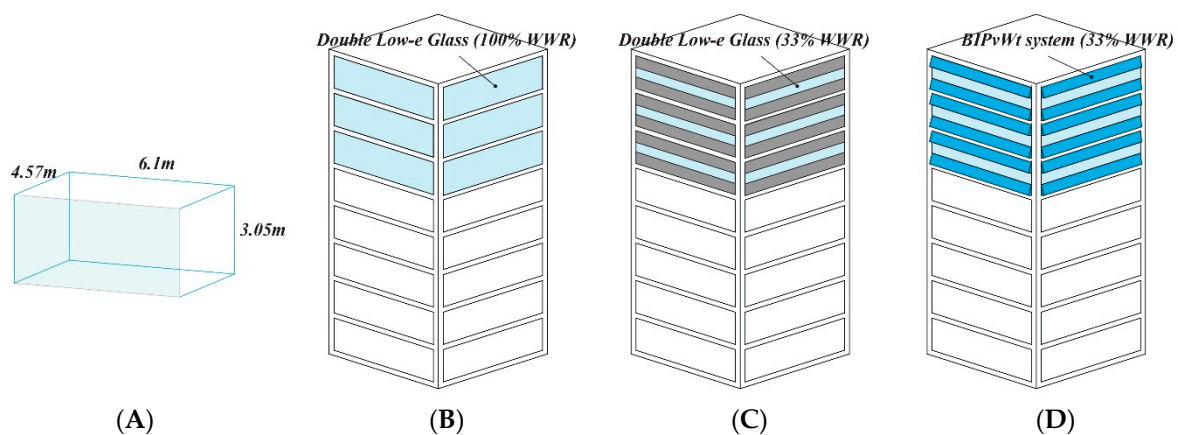


**Figure 2.** Building module prototype for the energy simulation. (A) Detailed unit drawing; (B) basic module (b1); (C) basic module2 (b2); (D) building-integrated photovoltaic and wind turbine (BIPvWt) module (BI).

Tables 1–3 list the other calculation assumptions, such as the infiltration and operation schedules. A 27.9 m<sup>2</sup> (300 ft<sup>2</sup>) space is available for each person in the office building under consideration [28]. Based on this, the internal loads for the equipment were calculated to be 8.07 W/m<sup>2</sup> (0.75 W/ft<sup>2</sup>) peak load. The sensible load per person was 297 W, which is 8.07 W sensible/m<sup>2</sup> (0.75 W sensible/ft<sup>2</sup>). As a lighting control, the calculation data was set with a constant lighting level of 538 lx by continuous dimming [13,29].

**Table 1.** Set point temperature for cooling (°C).

Time	Weekday	Saturday	Sunday
06:00–18:00	24	24	27
18:00–22:00	24	27	27
22:00–06:00	27	27	27

**Table 2.** Set point temperature for heating (°C).

Time	Weekday	Saturday	Sunday
06:00–18:00	21	21	16
18:00–22:00	21	16	16
22:00–06:00	16	16	16

**Table 3.** Infiltration schedules (at 0 pa).

Time	Weekday	Saturday	Sunday
06:00–18:00	0.25	0.25	1
18:00–22:00	0.25	1	1
22:00–06:00	1	1	1

### 2.3. BIPvWt System and Performance Efficiency

Park et al. [43] proposed a BIWT module utilizing a building skin. The BIWT module consisted of a rotor and a guide vane, which is the key composition that changes the approaching wind conditions, such as low velocity or high static pressure, to be appropriate for rotor operation. The proposed BIPvWt system, which is shown in Figure 3A, replaces a part of the guide vane with a silicon based PV. To determine the general form of the wind turbine system, the rotating direction of the rotor and the number and shape of the blades are considered using CFD analyses [43,49,50]. The rotor's total power coefficient, including generator efficiency, was 0.149 [43]. In addition, a silicon cell PV system installed on the guide vane can generate  $P_{\max}$  300 Wp/module with a 15% conversion efficiency. As an application, the BIPvWt system covers 30% of the upper bound of the building envelope because the approaching wind speed is faster in that region. The width and height of a unit module were 1.5 m (5 ft) to apply them easily to one perimeter zone.

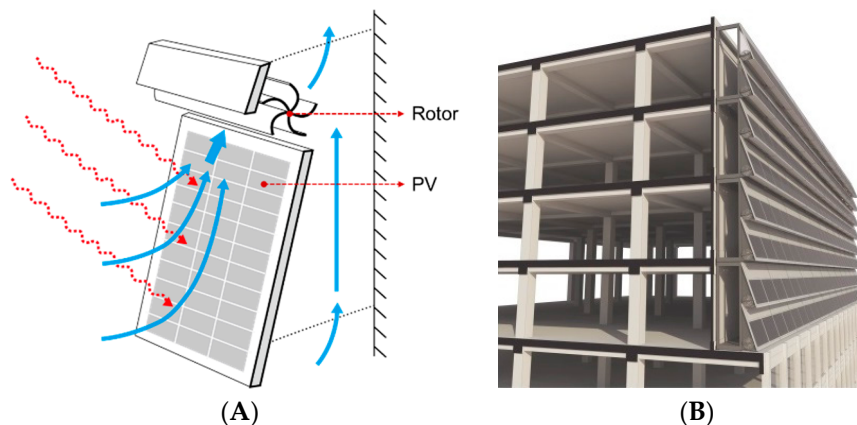


**Figure 3.** Diagram of the proposed BIPvWt system. (A) Detailed BIPvWt system drawing; (B) building envelope installation of BIPvWt.

Using the attached BIPvWt, it might work as a double skin façade. In the inside of the cavity space between the glass and external BIPV, 1.5 m gap, the air is accelerated, which might decrease the cooling load when it is ventilated [51,52]. In addition, the external additional skin provides an insulation effect by increasing the external heat transfer resistance. According to recent field studies [53–55], a properly installed double skin façade reduces the building energy load by 10% to 40% of the original energy consumption. Therefore, the proposed BIPvWt system can reduce the energy consumption more than expected, even though the current simulation does not fully support the effects of the double skin façade on the ventilation effect for the cooling load.

### 2.4. CFD Analyses and Calculation Assumptions for Wind Turbine

Full-scale CFD analyses were conducted to examine the performance of each module installed on the target building. Modelling the entire proposed system including the rotor takes a long time, so only the guide vane part was considered for the simulation. The differential pressure coefficient was calculated by measuring the undisturbed outlet velocity magnitudes of each module. Owing to the symmetric shape of the installed system, the results of the two models, whose wind-approaching angle

is  $\theta$  and  $-\theta$ , are also symmetric so one of them can replace another. For that reason, three different angles of incidence ( $0^\circ$ ,  $22.5^\circ$ , and  $45^\circ$ ) were considered to reduce the number of analysis cases [56].

The power production of the wind turbines of a BIPvWt system applied to a building envelop was estimated by the annual wind data from selected cities. The wind rose data were fitted using the Weibull distribution, which is a good fit to the measured wind speed data [57], for each wind direction [58,59]. In addition, the applied system was assumed to generate electric power from the approaching wind within an angle of  $90^\circ$ . For example, the system installed in a northward direction is affected by wind from the northeast, north-northeast, north, north-northwest, and northwest azimuths. Finally, the total power production of the applied system installed towards the  $\varphi$  direction can be written as the sum of the power converted from five different approaching wind directions as follows:

$$\text{Power}_{\varphi,\text{total}} = \text{Power}_{\varphi,-45^\circ} + \text{Power}_{\varphi,-22.5^\circ} + \text{Power}_{\varphi,0^\circ} + \text{Power}_{\varphi,22.5^\circ} + \text{Power}_{\varphi,45^\circ} \quad (1)$$

### 3. Results and Discussion

The results are divided into two parts: energy potential analysis in multiple urban areas and energy balance evaluation in selected cities. In the first part, as shown in the Appendix A, the energy potential can be compared according to the variation of global cities, which have their own climate patterns. Second, a feasibility test was performed by analyzing the energy consumption and generation in an office module in a specific building.

#### 3.1. Solar and Wind Energy Potential in Urban Area

The solar and wind energy generation potential based on the solar irradiation and wind speed and direction were analyzed. A unit, relative ratio (average value: 1.00), was used to compare the renewable energy potential. The climate data of 142 cities were considered to represent the energy generation in a typical major city. For example, the average value was calculated based on the data from 142 targeted cities among a total 1042 locations, which is provided in the weather data set. A relative ratio of 1 means that the city has an average value of the 142 cities. Therefore, the average level of solar irradiation and wind speed in each city was selected as 1. If the value is greater than 1, there is a high potential for energy generation. Conversely, if the value is less than 1, there is a low potential of energy generation. Initially, the solar and wind energy potentials were compared by the ASHRAE international climate classification to determine the regional similarity and difference in each energy potential. As shown in Figure 4, the solar energy potential showed some analogy in the same climate classification compared to the wind case. These results can be explained by the characteristics of the ASHRAE standard, which originate from the division of the thermal and humidity criteria [44]. In the wind energy cases, however, the variation is dispersed irregularly in a similar climate or adjacent cities.

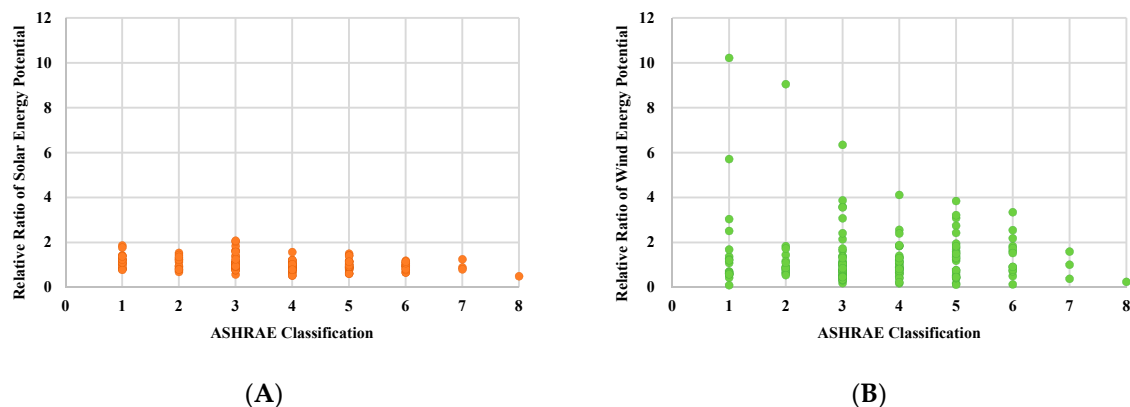


**Figure 4.** Energy potential according to the ASHRAE classification. (A) Solar energy potential; (B) wind energy potential.

Based on the energy potential data set, Table 4 and Figures 5 and 6 provide a statistical summary and a diagram of the distribution of the solar and wind energy potential, respectively. In addition, the basic abbreviated terms are the maximum value (Max), minimum value (Min), average value (AVG), and standard deviation (S.D.). In the case of Wellington, New Zealand, its energy potential has a maximum value (total: 2.25, solar: 0.97, and wind: 3.53), which has common characteristics in a wind dominated region (average wind energy potential in Australia is 1.15 and New Zealand is 2.31). On the other hand, in the case of Chongqing located in China, its potential has a minimum value (total: 0.31, solar: 0.47, and wind: 0.15), which can explain the regional features of a basin.

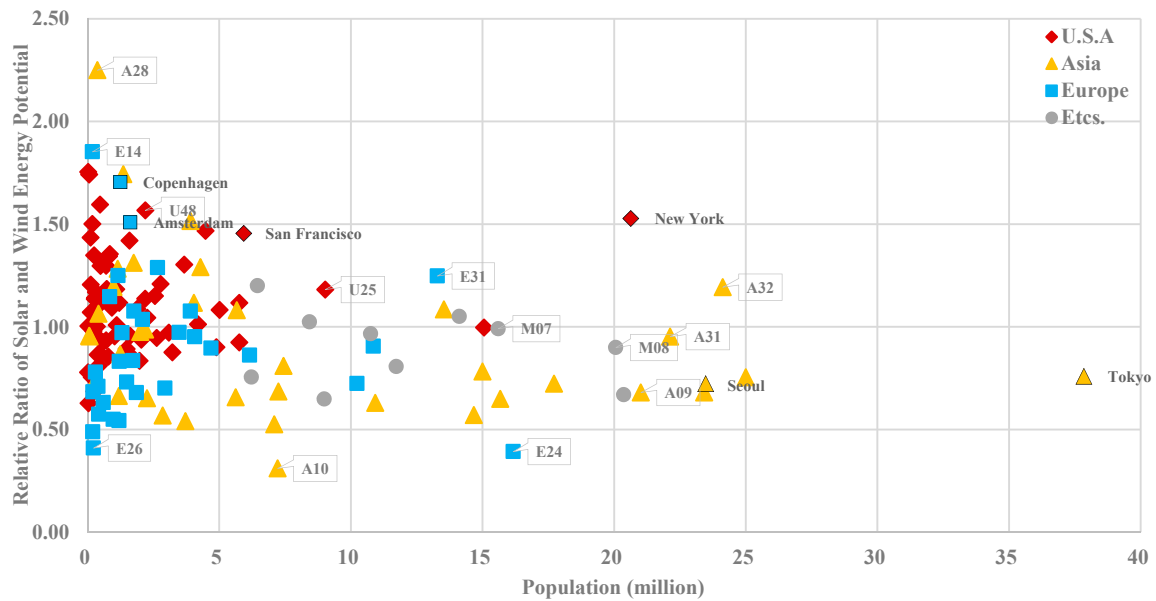


**Figure 5.** Total energy potential of the solar and wind source in global regions according to the population (see Appendix A for a more comprehensive list of abbreviations).

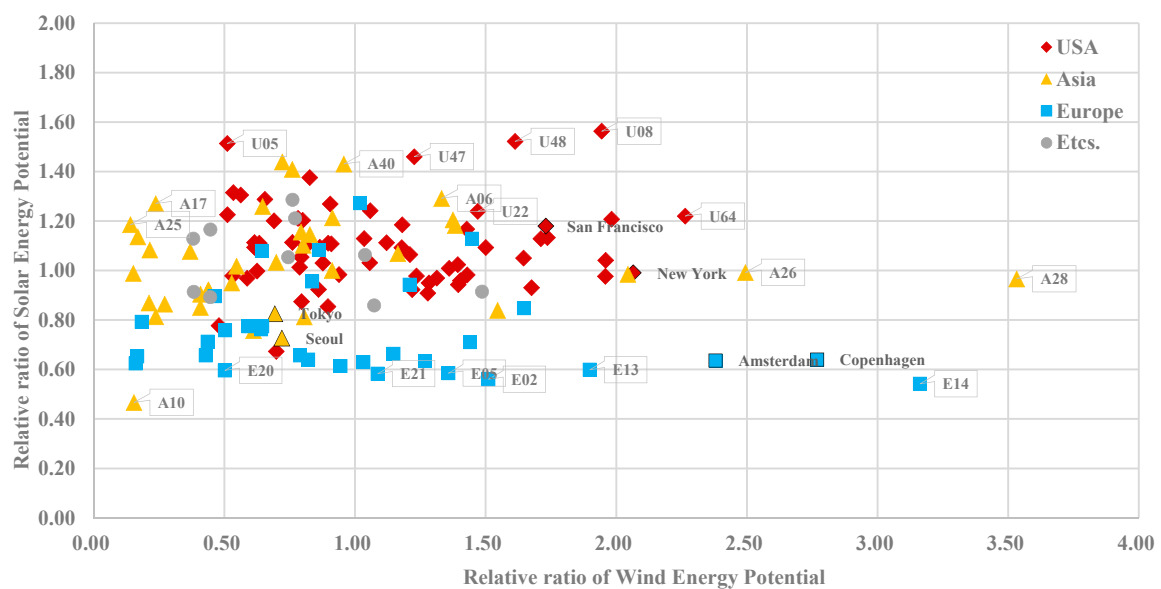


**Figure 6.** Solar and wind energy potential in global regions (see Appendix A for a more comprehensive list of abbreviations).

**Table 4.** Statistical summary of the relative renewable energy potential.

Region	Total (Solar + Wind)				Solar				Wind				Samples
	Max	Min	AVG	S.D.	Max	Min	AVG	S.D.	Max	Min	AVG	S.D.	
U.S.	1.75	0.63	1.11	0.25	1.56	0.67	1.10	0.17	2.26	0.48	1.12	0.46	63
Asia	2.25 <sup>1</sup>	0.31 <sup>2</sup>	0.92	0.37	1.44	0.47 <sup>2</sup>	1.03	0.21	3.53 <sup>1</sup>	0.14	0.81	0.69	38
Europe	1.85	0.39	0.91	0.35	1.27	0.54	0.75	0.19	3.16	0.16	1.06	0.72	32
Others	1.20	0.65	0.90	0.18	1.29	0.86	1.05	0.15	1.49	0.38	0.75	0.36	10
Total		-		0.32		-		0.23		-		0.60	143

<sup>1</sup> Wellington, <sup>2</sup> Chongqing.

In terms of data analysis based on the solar irradiation and wind speed, cities in the U.S. have a relatively high average (AVG) value than other regions. AVG in U.S. is 1.11, which has a high solar and wind energy potential; cities in Asia and Europe have an AVG value of 0.92 and 0.91, respectively. Cities in Asia are low wind speed cities, which have a 0.81 AVG value in wind energy potential. In cities in Europe, however, the wind energy potential (1.06 AVG value) is dominant compared to the solar energy potential (0.75 AVG value).

From the point of view of deviation, there are differences between the solar and wind energy potential. The standard deviation (S.D.) in solar energy is in the range, 0.17, 0.21, and 0.19, and the wind energy is in the range, 0.46, 0.69, and 0.72, respectively. Those distinctions can explain why the wind direction and speed are much more random and highly erratic compared to the solar case [60].

Among the three exemplary regions, two cities representative of the population and high-energy potential were selected and are marked in Figures 5 and 6. Table 5 lists the potential data for the six cities chosen. The main criteria for cities selection are (1) the relative range of energy potentials are between 0.7 and 1.5, which are lower 15% and upper 15% bound, and (2) large population and high density are the main consideration for future energy demand. In the next part, the detailed energy simulations in specific cities were tested based on the energy potential data source.

**Table 5.** Description of the six targeted cities for a detailed simulation.

City	Area (km <sup>2</sup> )	Population (Thousands)	Density (people/km <sup>2</sup> )	Relative Energy Potential			ASHRAE Classification
				Total	Solar	Wind	
New York City	11,642	20,630	1800	1.53	0.99	2.06	4A
San Francisco	2797	5929	2100	1.45	1.18	1.73	3C
Tokyo-Yokohama	8547	37,843	4400	0.76	0.83	0.69	4A
Seoul-Incheon	2266	23,480	10,400	0.72	0.73	0.72	4A
Copenhagen	453	1248	2800	1.70	0.64	2.77	5C
Amsterdam	505	1624	3200	1.51	0.64	2.38	4A

### 3.2. Building Energy Balance Simulation in Specific Office Module in Global Urban Areas

Six cities, which are listed in Table 5, (A) New York City (N.Y.), (B) San Francisco (S.F.), (C) Tokyo-Yokohama (Tokyo), (D) Seoul-Incheon (Seoul), (E) Copenhagen, and (F) Amsterdam, were simulated to compare the energy balance of the building modules. First, in the part of solar and PV, the variation of the angle of incidence and its effects on energy generation were examined. In terms of the exterior design, solar panels installed parallel to the elevation can have an integrated design and a sophisticated feel. On the other hand, the PV angle of incidence can also vary the input wind speed as well as the efficiency of the PV. Figure 7 shows the results of the PV angle and its energy generation. Based on the data from six cities, the optimal angle in the PV output might be in the range of 30 to 45° of the roof side. In addition, the reduction ratio in energy generation at a 90° angle of the roof side compared to the best performance angle (30° of the roof side) appears to be an average of 24.4% (21% to 30%). PV energy production is closely related to the climatic conditions, and it tends to be proportional to the solar irradiance. For example, in the case of an angle of 67.5° from the roof, the PV energy output is approximately 8.24 kWh/(m<sup>2</sup>·y) (San Francisco), 6.57 kWh/(m<sup>2</sup>·y)

(New York), 5.7 kWh/(m<sup>2</sup>·y) (Tokyo), 5.42 kWh/(m<sup>2</sup>·y) (Seoul), 4.68 kWh/(m<sup>2</sup>·y) (Amsterdam), and 4.29 kWh/(m<sup>2</sup>·y) (Copenhagen), respectively. This shows that the energy production can vary by up to 1.92 times using the same module within different climate conditions.

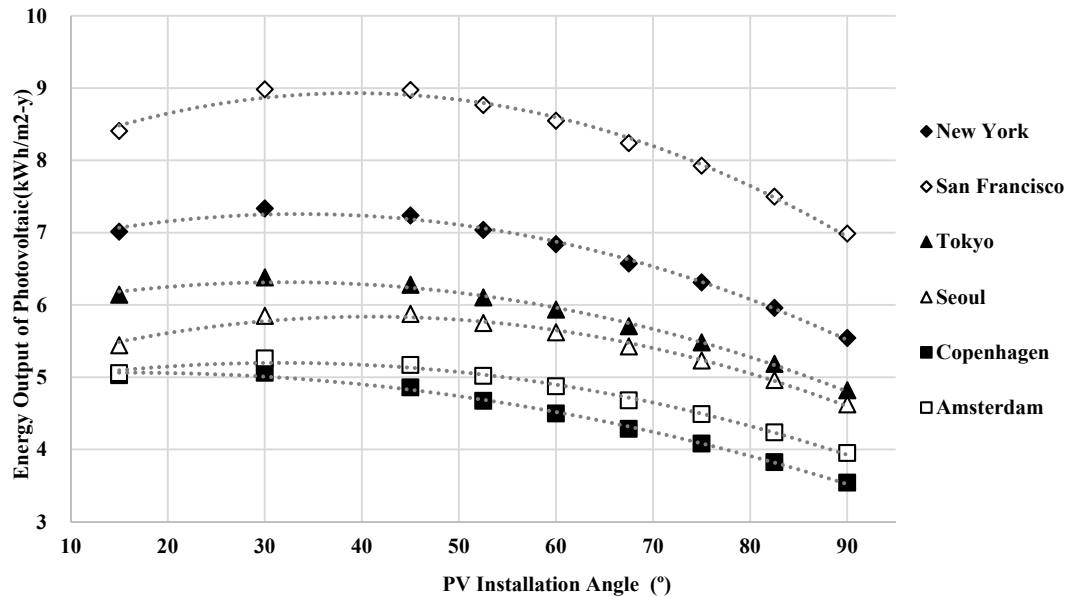


Figure 7. Photovoltaics (PV) energy output according to the envelope angle.

Solar irradiation has a decisive influence on PV energy production. Figure 8 shows the yearly energy output of PV by global horizontal irradiance based on an energy simulation of the 90° angle of a roof side PV application. According to the data, the energy outputs have a linear relationship according to the change in solar irradiation, which suggests that comparing the solar energy potential with solar irradiation is an appropriate method.

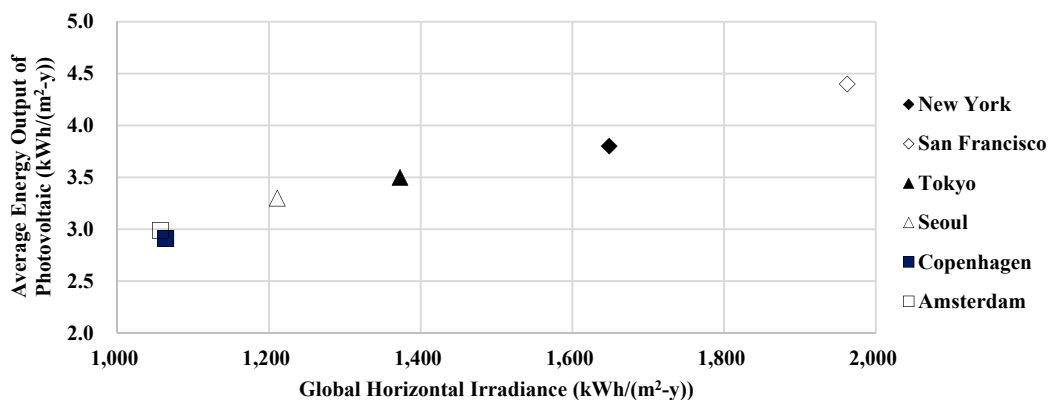
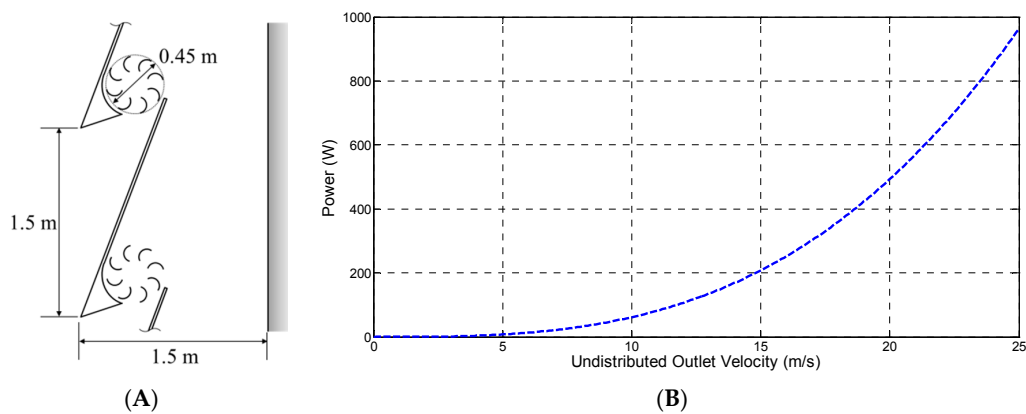
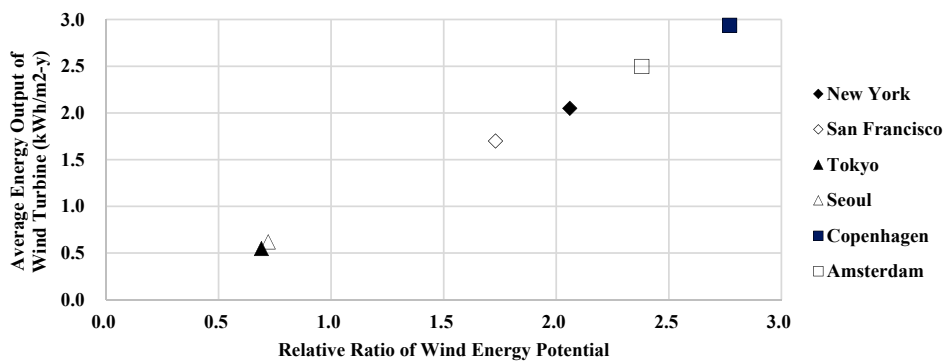


Figure 8. Annual average PV energy output as a function of the solar irradiation.

In the case of the wind related data, Figure 9 shows the generated power output of a wind turbine performed by a wind tunnel test. As the inlet velocity increases, the energy generation of a wind turbine is intensified. Figure 10 presents the yearly energy output of a wind turbine by the wind related climate data, such as speed and direction. According to the graph, to some extent, the energy output has a linear relationship with the change in wind climate data, which suggests that a comparison of the wind energy potential with the wind speed and direction is an appropriate method.



**Figure 9.** Power coefficient according to the wind turbine types [43]. (A) Sectional diagram of the wind turbine; (B) The generated power output of the wind turbine.



**Figure 10.** Annual average wind energy output as a function of the wind potential.

Evaluating the energy consumption and generation output by the application of a BIPvWt system in building envelope differs according to the climate conditions and building design and type. The energy output from the office buildings in the six selected cities was analyzed, as shown in Table 6 and Figure 11. The energy generation by PV and wind power differs according to the orientation that the building is facing. In addition, the energy consumption (heating, cooling, and lighting energy load) are different in terms of orientation and building material. In this evaluation, eight different orientations (South East, SE; South, S; South West, SW; West, W; North West, NW; North, N; North East, NE; and East, E) and three different types of envelopes (b1, Basic module; b2, Basic module2; and BI, BIPvWt module) in the six selected cities (N.Y., S.F., Tokyo, Seoul, Copenhagen, and Amsterdam) were simulated and drawn as a graph. In Figure 11, “+” in the  $y$  axis stands for the energy consumption, and “-” stands for the energy generation.

**Table 6.** Statistical description of energy consumption and generation in the six cities (kWh/(m<sup>2</sup>·y)).

City	Energy Consumption						Energy Generation				Total	
	Lighting		Heating		Cooling		PV		Wind			
	AVG <sup>1</sup>	S.D. <sup>2</sup>	AVG	S.D.	AVG	S.D.	AVG	S.D.	AVG	S.D.	AVG	S.D.
N.Y.	12.9	2.1	9.8	8.5	29.9	10.7	-3.8	1.6	-2.1	1.1	49.7	14.0
S.F.	12.0	1.8	0.5	0.9	6.5	4.0	-4.4	2.0	-1.7	1.8	16.0	5.4
Tokyo	13.1	1.8	6.6	6.6	21.7	6.8	-3.5	1.5	-0.6	0.3	39.4	9.8
Seoul	12.6	2.1	15.7	10.8	19.8	5.6	-3.0	1.4	-0.6	0.2	46.2	12.7
Copenhagen	15.2	2.4	19.0	12.9	2.7	1.4	-2.9	1.2	-2.9	2.2	34.0	14.3
Amsterdam	14.5	2.6	11.7	9.2	4.6	2.2	-3.0	1.3	-2.5	1.9	28.1	10.4

<sup>1</sup> Average, <sup>2</sup> Standard deviation.

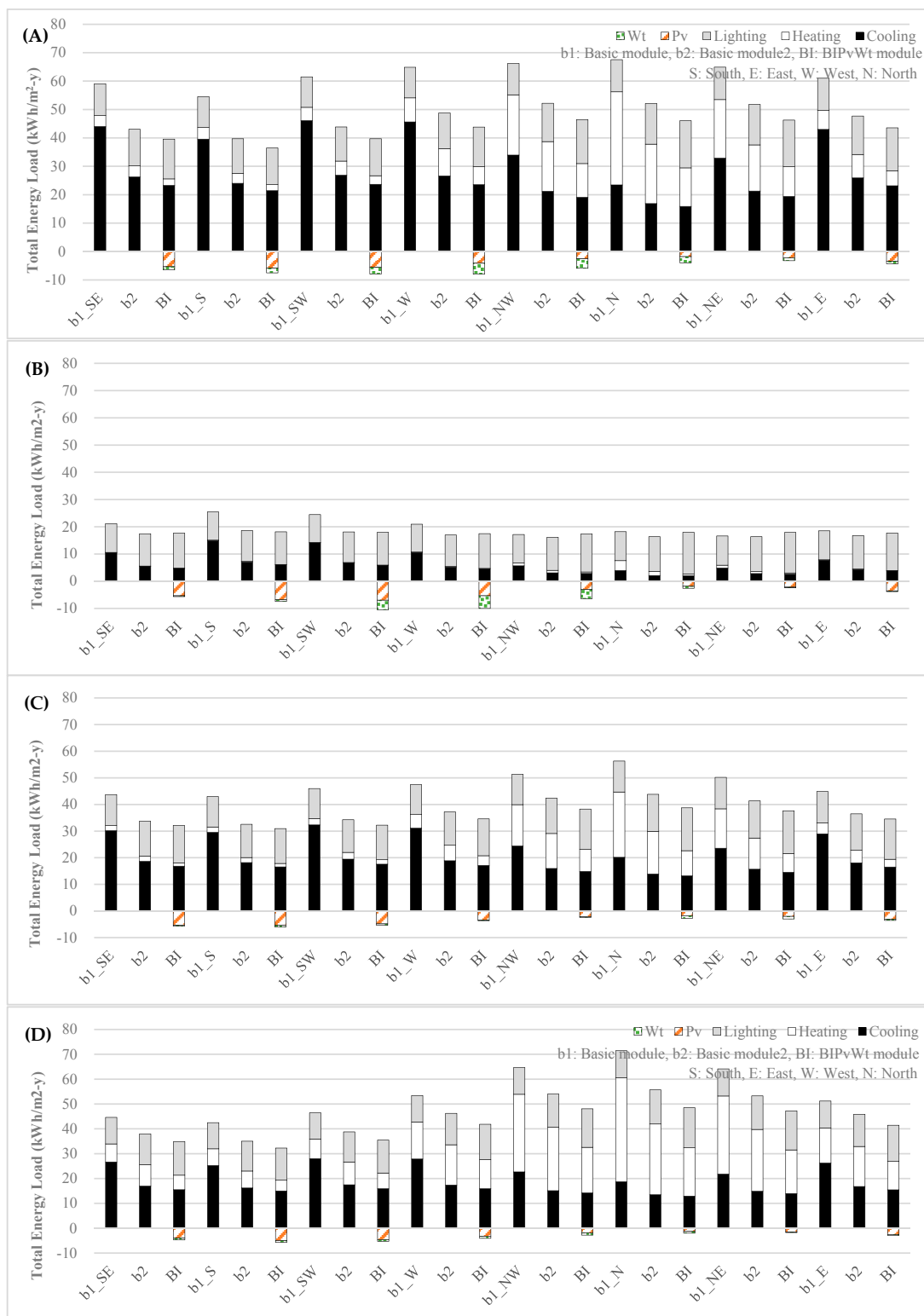
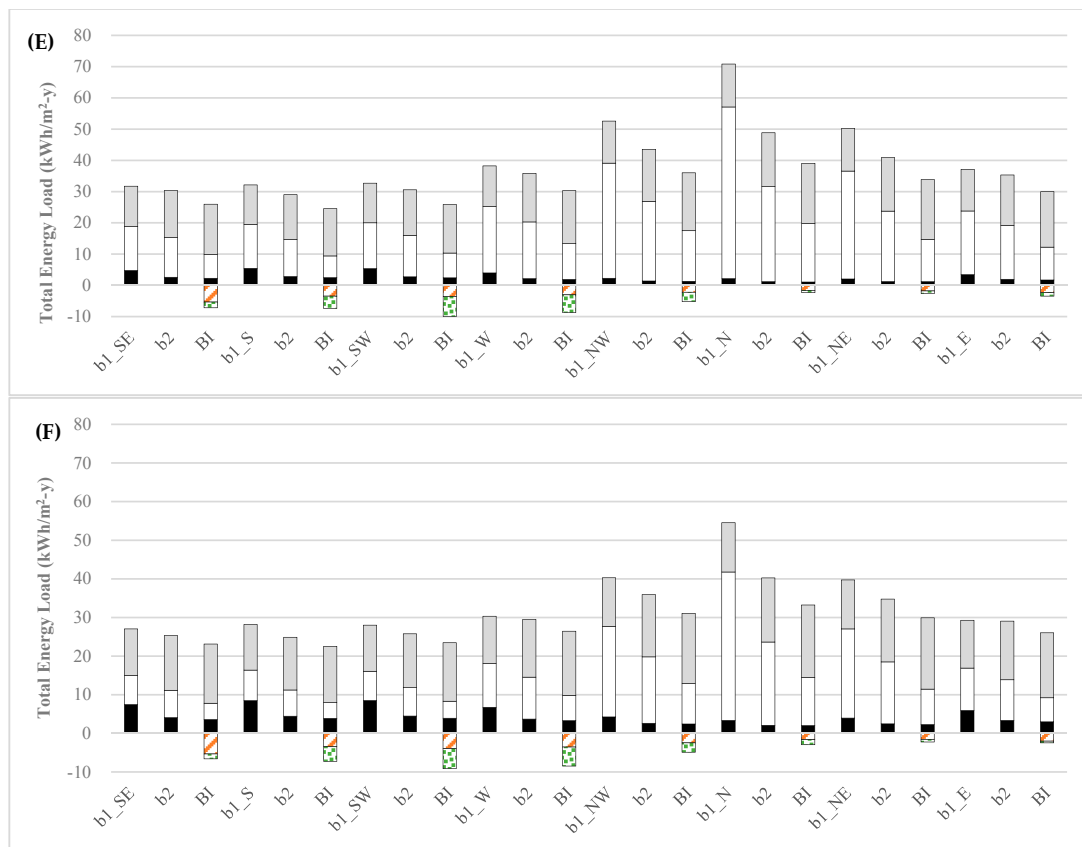


Figure 11. Cont.



**Figure 11.** Chart of the energy consumption and generation according to the orientation. (A) New York City, (B) San Francisco, (C) Tokyo-Yokohama, (D) Seoul-Incheon, (E) Copenhagen, and (F) Amsterdam.

The experimental results are presented in the following order: total energy consumption, WWR changes, orientation effect, total energy balance with PV, and wind energy generation. Before that, details and a thorough investigation of N.Y. was performed. N.Y. has the largest area, with a population ranked 8th and population density ranked 76th in the 142 target cities. PV and wind energy potential occupy a considerably higher 9th place. Hence, installation of the proposed BIPvWt system will have a considerable influence. Based on the average energy data shown in Figure 11, the cooling, heating, and lighting energy consumption ratios were estimated to be 20%, 55%, and 25%, respectively. When the proposed system is installed, it is expected it will not only reduce the energy consumption by approximately 25% as the WWR is lowered, but also produce energy reserves of up to 32% in terms of 3.8 kWh/(m<sup>2</sup>·y) in PV and 2.05 kWh/(m<sup>2</sup>·y) in wind energy generation. On the other hand, this shows a large deviation for each orientation. For example, the north orientation consumes the most energy and the south the least, with a ratio of approximately 1:0.79. In particular, the difference in heating energy consumption in relation to the orientation is significant (approximately 22.4 kWh/(m<sup>2</sup>·y) in the north orientation, and 3.23 kWh/(m<sup>2</sup>·y) in the south orientation). The difference in energy consumption according to the orientation requires further consideration in building design and renovation. In addition, the west and southwest are the most efficient in energy production, which can replace approximately 18% and 20% of the building energy consumption, respectively. Overall, significantly different results can be obtained in terms of energy consumption and generation depending on where the office is placed, how the layout is organized, and whether the proposed system is installed.

In the total energy consumption, the portion of the cooling and heating loads in the buildings in S.F., which have relatively small needs, had the lowest energy balance (16.0 kWh/(m<sup>2</sup>·y)) among the cities tested. On the other hand, the buildings in N.Y. required the highest total energy output

(49.7 kWh/(m<sup>2</sup>·y)) because the N.Y. case consumes considerable energy in cooling and heating. Although 4 cities without S.F. (3C) and Copenhagen (5C) are in a similar climate classification (4A) based on the ASHRAE (Table 5), the absolute total energy consumption, and the fact that the ratio between heating, cooling, and lighting energy vary in each city. In addition, depending on the region, the dominance of heating, cooling, and lighting may be different. Of the data in Figure 11, the ratio of energy usage is compared using the mean value of 100% (b1) and 33% (b2) WWR. For example, cooling is relatively dominant in N.Y. (approximately 56% of the total, up to 75%), lighting is relatively dominant in S.F. (approximately 60% of the total), cooling is slightly dominant in Seoul and Tokyo (approximately 40% and 52% of the total), while heating is dominant in Copenhagen and Amsterdam (approximately 57% and 44% of the total, up to 75%). This can vary depending on the changes in input parameters, such as building type, orientation, and HVAC (heating, ventilation, and air-conditioning) schedule. In particular, the ratio may vary significantly depending on orientation of the same area, indicating that the role of orientation in building design and layout can be considerable.

When the WWR changes from 100% to 33%, all cases showed that both the heating and cooling loads decrease and the lighting load increases. On the other hand, the total energy consumption decreases, because the plus amount of heating and cooling load is far outweighed compared to the minus amount of lighting load. As the WWR decreases from 100% (b1) to 30% (BI), 44.8% of the heating, cooling, and lighting load is decreased in the north of the Copenhagen area and 28% is decreased in the south of S.F. In other regions, a 39% (Amsterdam, northeast), 32.1% (Seoul, north), 28.6% (Tokyo, north), and 35.4% (N.Y., southwest) decrease in energy is observed when the WWR changes. This may be characterized by the interaction between the general climatic conditions (temperature or irradiation) and heating or cooling. In other words, in S.F., where the cooling is dominant, energy losses are reduced greatly in relation to the south, and in Copenhagen and Amsterdam, where the heating is dominant, the energy losses are influential in the north. Between cases “b2” and “BI”, they have the same condition of WWR, but there is an additional attachment of the BIPvWt system, which strengthens the thermal performance, and there are also some shading effects of the BIPvWt system. Therefore, most cases show a decrease in total energy consumption, except for S.F., which has a mild climate (3C in the ASHRAE classification) compared to other cities. In the case of S.F., in some cases, “BI” consumes more energy compared to “b2”, which is explained by the shading effect of the additional installation.

From an orientation and energy consumption point of view, six cities showed common results. A south and southeast (SE) facing building consumes the least energy, but a north-oriented building requires the highest energy load because the heating energy loads in the six cities increase considerably. In addition, the deviation in N.Y. (14.0) and Copenhagen (14.3) far outweighs the other cities. In the case of N.Y., the effects of a BIPvWt installation on reducing the energy loads is significant because the WWR changes from 100% to 33%. On the other hand, in the case of Copenhagen, the deviation in each orientation is critical and highlights the need for careful consideration in an urban layout in the design guideline. Tokyo and Seoul, which show opposite aspects in south and north orientations, require discreet analysis in heating and cooling control.

In the case of PV energy generation, most cities tend to generate much more energy in a south-related face installation and the trend of the distribution is commonly predictable. In addition, in a detailed point of installation, the PV output can cover at least 3.9% (N.Y., north orientation) and at most 37.6% (S.F., south orientation) of the total energy consumption.

In the case of wind energy generation, the trend of the distribution appears to be irregular and varies according to the city and orientation. Therefore, in a detailed point of installation, the wind energy output can cover at least 0.8% (Seoul, northeast orientation) and at most 26.5% (S.F., west orientation) of the total energy consumption. In addition, compared to the PV cases, most cities have a relatively large standard deviation in each orientation, which explains why the wind direction and speed are much more random and highly erratic compared to the PV cases.

The total energy balance results show that each city can cover the following proportion of its energy consumption as an application of the BiPvWt system in average value: N.Y., 14.4%; S.F., 38.0%; Tokyo, 11.8%; Seoul, 8.9%; Copenhagen, 21.0%; and Amsterdam, 22.4%. Given the energy potential data, which ranges from 0.72 to 1.70 (Table 5), most urban areas may reduce their energy consumption briefly by approximately 8–38% after applying the BiPvWt system. Therefore, as a design guideline, a south facing layout of the energy consumption and PV output is required. On the other hand, the distribution of wind speed and direction differs from most cities and the urban layout even causes differences in the wind energy potential. Therefore, careful consideration and computer-aid approaches, such as CFD analysis, are needed to identify the most suitable turbine location prior to installation.

#### 4. Conclusions

A feasibility simulation that evaluates a BiPvWt system in global regions was developed. The BiPvWt system can lead to a balance of the building energy consumption. The main findings can be summarized as follows:

- The solar and wind energy potential shows a range of distributions in global 143 regions and a diagram of the distribution of the solar and wind energy potential is plotted. In 143 cities, the deviation of the energy potential ranges from 0.31 to 2.25.
- The ASHRAE climate classification can explain the solar energy potential, but the wind energy potential, which includes speed and direction, shows relationships in similar regions or climate conditions.
- As a design guide or engineering suggestion, arranging office buildings in south-related installation is effective for heating and cooling. In a PV installation, the south-related faces are much more efficient than the north-related faces. In the six cities simulated, the PV energy output varies approximately twofold at most depending on the region that is largely affected by the climate conditions, such as solar irradiation. On the other hand, the wind direction and speed in the six targeted cities follow the regional and seasonal conditions, which suggests that careful consideration and installation are feasible.
- The BiPvWt system can cover 8–38% of the building energy consumption and has a leading advantage in energy saving in urban areas. In addition, as the WWR decreases from 100% to 30% through the application of BiPvWt, the heating, cooling, and lighting load decreases by 44.8% in the north of Copenhagen, 39% in the northeast of Amsterdam, 35.4% in the southwest of N.Y., 32.1% in the north of Seoul, 28.6% in the north of Tokyo, and 28% in south of S.F., respectively. As the proposed BiPvWt system is applied to the building envelope, there are many design considerations as well as a performance effect. Above all, the design will be similar to the BiPV system currently attached to the envelope. On the other hand, as there is a wind turbine inside the proposed system, additional factors, such as noise, weight, structural load, and vibration, will be need to be taken into account. Therefore, the design development of a BiPvWt and building design should be considered carefully along with building layout and enclosure design. This will also need to be considered in the future.
- The coverage ratio is expected to increase with the development of PV and wind turbine technology and optimized building energy consumption, which suggests engineering and technological development of those systems. Also, generalization was needed for this study in order to view the overall energy potential in various regions and to review the feasibility of the proposed system, and therefore the target building was set to the highest skyscraper. The main reason for this is that if we set up a normal building in the simulations, there are various problems that can occur within the city. For example, shadows can be created and wind speeds may vary depending on the building layout or blocking by other buildings. In addition, considering that high-rise buildings are built inside the city center, the shadow of other structures and horizontal

motion by wind can have a significant impact on the PV or wind energy production, which will be examined in a future study.

- The total energy consumption will have the most significant impact on the energy contribution of the proposed PV and wind integration system. Therefore, the energy consumption ratios may vary according to how the input parameters, such as the building type, orientation, and HVAC (heating, ventilation, and air-conditioning) schedule, are set. Accordingly, it is important to select the appropriate input parameters. In addition, various design guidelines for urban areas have been released based on the local climate and building types; however, after careful consideration of potential renewable energy applications, building and urban design guidelines can be developed and harmonized based on the energy related fields.

**Acknowledgments:** This work was supported by INHA UNIVERSITY Research Grant.

**Author Contributions:** Jaewook Lee and Jeongsu Park has designed and written the manuscript under the supervision of Hyung-Jo Jung and Jiyoung Park. All authors have read and approved the final manuscript.

**Conflicts of Interest:** The authors declare no conflict of interest. The founding sponsors had no role in the design of the study; in the collection, analyses, or interpretation of data; in the writing of the manuscript, and in the decision to publish the results.

## Appendix A. City Information and Energy Potential

No	Country	City	Area (km <sup>2</sup> )	Population (10 <sup>3</sup> )	Density (km <sup>2</sup> )	Total Potential *	Solar Potential *	Wind Potential *	ASHRAE Classification
A01	Australia	Adelaide	852	1140	1300	1.28	1.18	1.38	3C
A02	Australia	Brisbane	1972	1999	1000	0.97	1.16	0.79	2A
A03	Australia	Canberra	472	412	900	1.06	1.21	0.91	4A
A04	Australia	Darwin	216	73	300	0.95	1.26	0.65	1B
A05	Australia	Melbourne	2543	3906	1500	1.52	0.99	2.04	3C
A06	Australia	Perth	1566	1751	1100	1.31	1.29	1.33	3A
A07	Australia	Sydney	2037	4036	2000	1.12	1.07	1.16	3A
A08	Bangladesh	Dhaka	360	15,669	43,500	0.65	1.08	0.21	1A
A09	China	Beijing	3820	21,009	5500	0.68	0.92	0.44	4A
A10	China	Chongqing	932	7217	7700	0.31	0.47	0.15	3A
A11	China	Shanghai	3820	23,416	6100	0.68	0.92	0.44	3A
A12	China	Tianjin	2007	10,920	5400	0.63	0.85	0.41	4A
A14	China	Hong Kong	275	7246	26,400	0.68	0.76	0.61	2A
A15	India	Bombay	546	17,712	32,400	0.72	1.08	0.37	1B
A16	India	Calcutta	1204	14,667	12,200	0.57	0.99	0.15	1B
A17	India	Delhi	2072	24,998	12,100	0.75	1.27	0.24	1B
A18	Iran	Tehran	1489	13,532	9100	1.08	1.41	0.76	3B
A19	Japan	Tokyo-Yokohama	8547	37,843	4400	0.76	0.83	0.69	4A
A20	Kazakhstan	Semipalatinsk	210	299	1425	0.74	0.95	0.53	7
A21	Korea	Seoul-Incheon	2266	23,480	10,400	0.72	0.73	0.72	4A
A22	Kuwait	Kuwait City	712	4283	6000	1.29	1.21	1.37	1B
A23	Malaysia	Kuala Lumpur	1943	7088	3600	0.53	0.81	0.24	1A
A24	Mongolia	Ulaanbataar	233	1237	5300	0.87	1.03	0.7	7
A25	Nepal	Kathmandu	60	1180	19,800	0.66	1.19	0.14	3A
A26	New Zealand	Auckland	544	1356	2500	1.74	0.99	2.49	3C
A27	New Zealand	Rotorua	89	56	630	0.96	1	0.91	4A
A28	New Zealand	Wellington	184	370	2000	2.25	0.97	3.53	3C
A29	North Korea	Pyongyang	176	2850	16,200	0.57	0.87	0.27	5A
A31	Pakistan	Karachi	945	22,123	23,400	0.95	1.1	0.8	1B
A32	Philippines	Manila	1580	24,123	15,300	1.19	0.84	1.55	1A
A34	Saudi Arabia	Riyadh	1502	5666	3800	1.08	1.44	0.72	1B
A35	Singapore	Singapore	518	5624	10,900	0.66	0.91	0.41	1A
A37	Sri Lanka	Colombo	223	2180	9800	0.99	1.15	0.83	1A
A38	Taiwan	Taipei	1140	7438	6500	0.81	0.81	0.81	2A
A39	Thailand	Bangkok	2590	14,998	5800	0.78	1.02	0.55	1B
A40	United Arab Emirates	Abu Dhabi	881	982	1100	1.19	1.43	0.96	1B

No	Country	City	Area (km <sup>2</sup> )	Population (10 <sup>3</sup> )	Density (km <sup>2</sup> )	Total Potential *	Solar Potential *	Wind Potential *	ASHRAE Classification
A41	Uzbekistan	Tashkent	531	2250	4200	0.65	1.14	0.17	4C
A42	Viet Nam	Hanoi	466	3715	8000	0.54	0.87	0.21	1A
E01	Austria	Vienna	453	1763	3900	1.08	0.71	1.44	5A
E02	Belgium	Brussels	803	2089	2600	1.04	0.56	1.51	4A
E03	Bulgaria	Sofia	207	1195	5800	0.54	0.66	0.43	5A
E04	Bosnia and Herzegovina	Banja.Luka	1238	199	161	0.49	0.79	0.18	4A
E05	Czech Republic	Prague	285	1310	4600	0.97	0.59	1.36	5A
E07	Denmark	Copenhagen	453	1248	2800	1.7	0.64	2.77	5C
E08	Finland	Helsinki	641	1208	1900	0.83	0.63	1.03	6A
E09	France	Paris.Orly	2845	10,858	3800	0.91	0.66	1.15	4A
E10	Germany	Berlin	1347	4069	3000	0.95	0.63	1.27	5C
E11	Greece	Athens	583	3484	6000	0.97	1.08	0.86	3A
E12	Hungary	Debrecen	461	204	443	0.68	0.78	0.59	5A
E13	Ireland	Dublin	453	1160	2600	1.25	0.6	1.9	4A
E14	Iceland	Reykjavik	80	185	2300	1.85	0.54	3.16	6A
E15	Israel	Jerusalem	233	840	3600	1.15	1.27	1.02	3C
E16	Italy	Rome	1114	3906	3500	1.08	0.94	1.21	3C
E17	Italy	Venice	130	426	3300	0.57	0.71	0.44	4A
E18	Lithuania	Kaunas	157	301	1919	0.78	0.61	0.94	6A
E19	Netherlands	Amsterdam	505	1624	3200	1.51	0.64	2.38	4A
E20	Norway	Oslo.Fornebu	290	975	3400	0.55	0.6	0.5	6A
E21	Poland	Warszawa.Okecie	544	1720	3200	0.84	0.58	1.09	5A
E22	Portugal	Lisboa	1101	2661	2400	1.29	1.13	1.45	3C
E23	Romania	Bucharest	285	1860	6500	0.68	0.9	0.46	5A
E24	Russian Federation	Moscow	4662	16,170	3500	0.39	0.63	0.16	6A
E25	Slovakia	Bratislava	119	400	3400	0.71	0.77	0.65	5A
E26	Slovenia	Ljubljana	54	225	4100	0.41	0.65	0.17	5A
E27	Spain	Barcelona	1075	4693	4400	0.9	0.96	0.84	3C
E28	Spain	Madrid	1269	6155	4800	0.86	1.08	0.64	3C
E29	Sweden	Stockholm.Arlanda	382	1484	3900	0.73	0.64	0.82	6A
E30	Switzerland	Geneva	181	599	3300	0.63	0.76	0.5	4A
E31	Turkey	Istanbul	1360	13,287	9800	1.25	0.85	1.65	3C
E32	Ukraine	Kiev	544	2940	4100	0.7	0.76	0.64	5A
E33	United Kingdom	London	1738	10,236	5900	0.72	0.66	0.79	4A
U01	U.S.	AK Anchorage	220	251	1100	0.69	0.67	0.70	6A
U02	U.S.	AK Fairbanks	85	32	380	0.63	0.78	0.48	8
U03	U.S.	AL Birmingham	1373	790	600	0.85	1.09	0.62	3A
U04	U.S.	AR Little Rock	668	431	600	0.81	1.00	0.62	3A
U05	U.S.	AZ Phoenix	3196	4194	1300	1.01	1.51	0.51	2B
U06	U.S.	CA Arcata	28	18	622	0.78	0.97	0.59	4A
U07	U.S.	CA Bakersfield	357	590	1700	0.92	1.32	0.53	3B
U08	U.S.	CA Barstow-Daggett	107	23	210	1.75	1.56	1.94	2B
U09	U.S.	CA Fresno	443	703	1600	0.93	1.31	0.56	3A
U10	U.S.	CA Long Beach	133	469	3500	0.87	1.23	0.51	3A
U11	U.S.	CA Los Angeles	6299	15,058	2400	1.00	1.21	0.78	3C
U12	U.S.	CA Sacramento	1220	1885	1500	1.09	1.27	0.91	3C
U13	U.S.	CA San Diego	1896	3086	1600	0.97	1.29	0.65	3A
U14	U.S.	CA San Francisco	2797	5929	2100	1.45	1.18	1.73	3C
U15	U.S.	CO Denver	1730	2559	1500	1.15	1.24	1.06	5B
U16	U.S.	DC Washington	3424	4889	1400	0.90	1.01	0.79	0
U18	U.S.	FL Miami	3209	5764	1800	1.12	1.11	1.12	1A
U19	U.S.	FL Orlando	1958	2040	1000	0.94	1.11	0.76	2A
U20	U.S.	FL Tampa	2479	2621	1100	0.95	1.20	0.69	2A
U21	U.S.	GA Atlanta	6851	5015	700	1.08	1.13	1.03	3A
U22	U.S.	HI Honolulu	440	842	1900	1.35	1.24	1.47	1A
U23	U.S.	IA Des Moines	521	489	900	1.30	1.09	1.50	5A
U24	U.S.	ID Boise	347	350	1000	1.00	1.20	0.80	5B
U25	U.S.	IL Chicago	6856	9023	1300	1.18	0.96	1.40	5A
U26	U.S.	IN Fort Wayne	445	313	700	1.17	0.94	1.39	5A
U27	U.S.	KS Wichita	557	473	900	1.59	1.21	1.98	4A
U28	U.S.	KY Lexington	228	290	1300	0.96	0.98	0.94	4A
U29	U.S.	KY Louisville	1235	1025	800	0.95	1.03	0.88	4A
U30	U.S.	LA New Orleans	650	922	1400	1.09	0.91	1.28	2A
U31	U.S.	MA Boston	5325	4478	800	1.47	0.98	1.96	5A
U32	U.S.	MD Baltimore	1857	2263	1200	1.04	1.03	1.06	4A
U33	U.S.	MI Detroit	3463	3672	1100	1.30	0.93	1.68	5A
U34	U.S.	MN Duluth	181	120	700	1.21	0.98	1.43	7

No	Country	City	Area (km <sup>2</sup> )	Population (10 <sup>3</sup> )	Density (km <sup>2</sup> )	Total Potential *	Solar Potential *	Wind Potential *	ASHRAE Classification
U35	U.S.	MN Minneapolis-St. Paul	2647	2771	1000	1.21	1.02	1.39	6A
U36	U.S.	MO Kansas City	1756	1593	900	1.42	1.13	1.71	4A
U37	U.S.	MO Springfield	368	274	700	1.14	1.09	1.18	4A
U38	U.S.	MO St. Louis	2393	2186	900	1.14	1.06	1.21	4A
U39	U.S.	MS Jackson	627	380	600	0.86	1.11	0.62	3A
U40	U.S.	MT Billings	137	115	800	1.44	1.13	1.74	5B
U41	U.S.	MT Helena	42	30	666	1.00	1.11	0.90	6B
U42	U.S.	NC Charlotte	1919	1535	800	0.87	1.11	0.63	3A
U43	U.S.	NC Wilmington	347	220	600	0.98	1.09	0.87	3A
U44	U.S.	ND Fargo	181	177	1000	1.50	1.04	1.96	6A
U45	U.S.	NE Omaha	702	725	1100	1.18	1.01	1.36	5A
U46	U.S.	NJ Newark	63	278	4424	1.14	0.97	1.31	4A
U47	U.S.	NM Albuquerque	650	812	1200	1.34	1.46	1.23	4B
U48	U.S.	NV Las Vegas	1080	2191	2000	1.57	1.52	1.61	2B
U49	U.S.	NV Reno	425	392	900	1.10	1.38	0.83	5B
U50	U.S.	NY New York City	11,642	20,630	1800	1.53	0.99	2.06	4A
U51	U.S.	OH Columbus	1321	1481	1100	0.89	0.92	0.86	4A
U52	U.S.	OK Tulsa	870	702	800	1.30	1.17	1.43	4C
U53	U.S.	OR Portland	1357	1976	1500	0.84	0.87	0.80	4A
U54	U.S.	RI Providence	1412	1201	900	1.12	0.95	1.28	5A
U55	U.S.	TN Memphis	1287	1102	900	1.01	1.11	0.91	3A
U56	U.S.	TX Austin	1355	1616	1200	0.96	1.10	0.81	2A
U57	U.S.	TX Houston	4644	5764	1200	0.92	1.05	0.79	2A
U58	U.S.	UT Salt Lake City	720	1085	1500	1.18	1.19	1.18	5B
U59	U.S.	VA Norfolk	140	246	1733	1.35	1.05	1.65	3A
U60	U.S.	VT Burlington	233	120	500	1.07	0.92	1.22	6A
U61	U.S.	WA Seattle	2616	3218	1200	0.88	0.85	0.90	4A
U62	U.S.	WI Madison	391	402	1000	1.11	0.98	1.24	5A
U63	U.S.	WV Charleston	254	153	600	0.76	0.98	0.53	4A
U64	U.S.	WY Casper	71	58	794	1.74	1.22	2.26	6B
M01	Argentina	Buenos Aires	2681	14,122	5300	1.05	1.06	1.04	3A
M02	Brazil	Rio de Janeiro	2020	11,727	5800	0.81	1.17	0.45	1A
M03	Brazil	Sao Paulo	2707	20,365	7500	0.67	0.89	0.45	2A
M04	Canada	Toronto	2287	6456	2800	1.2	0.91	1.49	6A
M05	Chile	Santiago	984	6225	6300	0.76	1.13	0.38	3C
M06	Colombia	Bogota	492	8991	18,300	0.65	0.91	0.38	3C
M07	Egypt	Cairo	1761	15,600	8900	0.99	1.21	0.77	2B
M08	Mexico	Mexico City	2072	20,063	9700	0.9	1.05	0.74	3B
M09	Peru	Lima	919	10,750	11,700	0.97	0.86	1.07	2A
M10	South Africa	Johannesburg	2590	8432	3300	1.02	1.29	0.76	3C

\* each "potential" represents relative size to the average.

## References

1. United Nations Department of Economics and Social Affairs, Population Division. *World Urbanization Prospects: The 2014 Revision*; United Nations Publications: Herndon, VA, USA, 2015.
2. Deal, B.; Schunk, D. Spatial dynamic modeling and urban land use transformation: A simulation approach to assessing the costs of urban sprawl. *Ecol. Econ.* **2004**, *51*, 79–95. [[CrossRef](#)]
3. Ramesh, T.; Prakash, R.; Shukla, K.K. Life cycle energy analysis of buildings: An overview. *Energy Build.* **2010**, *42*, 1592–1600. [[CrossRef](#)]
4. Cabeza, L.F.; Rincón, L.; Vilarinho, V.; Pérez, G.; Castell, A. Life cycle assessment (LCA) and life cycle energy analysis (LCEA) of buildings and the building sector: A review. *Renew. Sustain. Energy Rev.* **2014**, *29*, 394–416. [[CrossRef](#)]
5. Colmenar-Santos, A.; Borge-Díez, D.; Rosales-Asensio, E. *District Heating and Cooling Networks in the European Union*; Springer: Cham, Switzerland, 2017.
6. Economidou, M.; Atanasiu, B.; Despret, C.; Maio, J.; Nolte, I.; Rapf, O. *Europe's Buildings under the Microscope. A Country-By-Country Review of the Energy Performance of Buildings*; Buildings Performance Institute Europe (BPIE): Bruxelles, Belgium, 2011.

7. Ochoa, C.E.; Aries, M.B.; Hensen, J.L. State of the art in lighting simulation for building science: A literature review. *J. Build. Perform. Simul.* **2012**, *5*, 209–233. [[CrossRef](#)]
8. Clarke, J.A.; Cockroft, J.; Conner, S.; Hand, J.W.; Kelly, N.J.; Moore, R.; O'Brien, T.; Strachan, P. Simulation-assisted control in building energy management systems. *Energy Build.* **2002**, *34*, 933–940. [[CrossRef](#)]
9. Crawley, D.B.; Lawrie, L.K.; Winkelmann, F.C.; Buhl, W.F.; Huang, Y.J.; Pedersen, C.O.; Glazer, J.; Strand, R.K.; Liesen, R.J.; Fisher, D.E.; et al. EnergyPlus: Creating a new-generation building energy simulation program. *Energy Build.* **2001**, *33*, 319–331. [[CrossRef](#)]
10. Caldas, L.G.; Norford, L.K. A design optimization tool based on a genetic algorithm. *Autom. Constr.* **2002**, *11*, 173–184. [[CrossRef](#)]
11. Kämpf, J.H.; Robinson, D. Optimisation of building form for solar energy utilisation using constrained evolutionary algorithms. *Energy Build.* **2010**, *42*, 807–814. [[CrossRef](#)]
12. Yi, Y.K.; Kim, H. Agent-based geometry optimization with Genetic Algorithm (GA) for tall apartment's solar right. *Sol. Energy* **2015**, *113*, 236–250. [[CrossRef](#)]
13. Dounis, A.I.; Caraiscos, C. Advanced control systems engineering for energy and comfort management in a building environment—A review. *Renew. Sustain. Energy Rev.* **2009**, *13*, 1246–1261. [[CrossRef](#)]
14. Lee, J.W.; Jung, H.J.; Park, J.Y.; Lee, J.B.; Yoon, Y. Optimization of building window system in Asian regions by analyzing solar heat gain and daylighting elements. *Renew. Energy* **2013**, *50*, 522–531. [[CrossRef](#)]
15. Sadineni, S.B.; Madala, S.; Boehm, R.F. Passive building energy savings: A review of building envelope components. *Renew. Sustain. Energy Rev.* **2011**, *15*, 3617–3631. [[CrossRef](#)]
16. Delgarm, N.; Sajadi, B.; Kowsary, F.; Delgarm, S. Multi-objective optimization of the building energy performance: A simulation-based approach by means of particle swarm optimization (PSO). *Appl. Energy* **2016**, *170*, 293–303. [[CrossRef](#)]
17. Hamdy, M.; Nguyen, A.T.; Hensen, J.L. A performance comparison of multi-objective optimization algorithms for solving nearly-zero-energy-building design problems. *Energy Build.* **2016**, *121*, 57–71. [[CrossRef](#)]
18. Nasar, J.L. Urban design aesthetics: The evaluative qualities of building exteriors. *Environ. Behav.* **1994**, *26*, 377–401. [[CrossRef](#)]
19. Ali-Toudert, F.; Mayer, H. Numerical study on the effects of aspect ratio and orientation of an urban street canyon on outdoor thermal comfort in hot and dry climate. *Build. Environ.* **2006**, *41*, 94–108. [[CrossRef](#)]
20. Kwok, A.G.; Grondzik, W.T. The green studio handbook: Environmental strategies for schematic design. *Enq. J. Archit. Res.* **2007**, *4*. [[CrossRef](#)]
21. Augenbroe, G. Integrated building performance evaluation in the early design stages. *Build. Environ.* **1992**, *27*, 149–161. [[CrossRef](#)]
22. Reinhart, C.F.; Mardaljevic, J.; Rogers, Z. Dynamic daylight performance metrics for sustainable building design. *Leukos* **2006**, *3*, 7–31.
23. Humphreys, M.A. Quantifying occupant comfort: Are combined indices of the indoor environment practicable? *Build. Res. Inf.* **2005**, *33*, 317–325. [[CrossRef](#)]
24. Boubekri, M.; Hull, R.B.; Boyer, L.L. Impact of window size and sunlight penetration on office workers' mood and satisfaction: A novel way of assessing sunlight. *Environ. Behav.* **1991**, *23*, 474–493. [[CrossRef](#)]
25. Connolly, D.; Lund, H.; Mathiesen, B.V.; Leahy, M. A review of computer tools for analysing the integration of renewable energy into various energy systems. *Appl. Energy* **2010**, *87*, 1059–1082. [[CrossRef](#)]
26. Yan, J.; Chou, S.K.; Desideri, U.; Tu, S.T.; Jin, H.G. Research, development and innovations for sustainable future energy systems. *Appl. Energy* **2013**, *112*, 393–395. [[CrossRef](#)]
27. Popescu, D.; Bienert, S.; Schützenhofer, C.; Boazu, R. Impact of energy efficiency measures on the economic value of buildings. *Appl. Energy* **2012**, *89*, 454–463. [[CrossRef](#)]
28. Agrawal, B.; Tiwari, G.N. Optimizing the energy and exergy of building integrated photovoltaic thermal (BIPVT) systems under cold climatic conditions. *Appl. Energy* **2010**, *87*, 417–426. [[CrossRef](#)]
29. Lee, J.W.; Park, J.; Jung, H.J. A feasibility study on a building's window system based on dye-sensitized solar cells. *Energy Build.* **2014**, *81*, 38–47. [[CrossRef](#)]
30. Quesada, G.; Guillon, L.; Rousse, D.R.; Mehrtash, M.; Dutil, Y.; Paradis, P.L. Tracking strategy for photovoltaic solar systems in high latitudes. *Energy Convers. Manag.* **2015**, *103*, 147–156. [[CrossRef](#)]

31. Antonanzas, J.; Urraca, R.; Martinez-de-Pison, F.J.; Antonanzas-Torres, F. Solar irradiation mapping with exogenous data from support vector regression machines estimations. *Energy Convers. Manag.* **2015**, *100*, 380–390. [[CrossRef](#)]
32. Xie, W.; Zeng, P.; Lei, L. A novel folding blade of wind turbine rotor for effective power control. *Energy Convers. Manag.* **2015**, *101*, 52–65. [[CrossRef](#)]
33. Xu, R.; Wittkopf, S.; Roeske, C. Quantitative Evaluation of BIPV Visual Impact in Building Retrofits Using Saliency Models. *Energies* **2017**, *10*, 668.
34. Hu, Z.; He, W.; Ji, J.; Hu, D.; Lv, S.; Chen, H.; Shen, Z. Comparative study on the annual performance of three types of building integrated photovoltaic (BIPV) Trombe wall system. *Appl. Energy* **2017**, *194*, 81–93. [[CrossRef](#)]
35. Sinha, S.; Chandel, S.S. Prospects of solar photovoltaic-micro-wind based hybrid power systems in western Himalayan state of Himachal Pradesh in India. *Energy Convers. Manag.* **2015**, *105*, 1340–1351. [[CrossRef](#)]
36. Nojavan, S.; Aalami, H.A. Stochastic energy procurement of large electricity consumer considering photovoltaic, wind-turbine, micro-turbines, energy storage system in the presence of demand response program. *Energy Convers. Manag.* **2015**, *103*, 1008–1018. [[CrossRef](#)]
37. Colantoni, A.; Allegrini, E.; Boubaker, K.; Longo, L.; Di Giacinto, S.; Biondi, P. New insights for renewable energy hybrid photovoltaic/wind installations in Tunisia through a mathematical model. *Energy Convers. Manag.* **2013**, *75*, 398–401. [[CrossRef](#)]
38. Sinha, S.; Chandel, S.S. Analysis of fixed tilt and sun tracking photovoltaic-micro wind based hybrid power systems. *Energy Convers. Manag.* **2016**, *115*, 265–275. [[CrossRef](#)]
39. Al Busaidi, A.S.; Kazem, H.A.; Al-Badi, A.H.; Khan, M.F. A review of optimum sizing of hybrid PV-Wind renewable energy systems in Oman. *Renew. Sustain. Energy Rev.* **2016**, *53*, 185–193. [[CrossRef](#)]
40. Agathokleous, R.A.; Kalogirou, S.A. Double skin facades (DSF) and building integrated photovoltaics (BIPV): A review of configurations and heat transfer characteristics. *Renew. Energy* **2016**, *89*, 743–756. [[CrossRef](#)]
41. Hassanli, S.; Hu, G.; Kwok, K.C.; Fletcher, D.F. Utilizing cavity flow within double skin façade for wind energy harvesting in buildings. *J. Wind Eng. Ind. Aerodyn.* **2017**, *167*, 114–127. [[CrossRef](#)]
42. Li, Q.S.; Shu, Z.R.; Chen, F.B. Performance assessment of tall building-integrated wind turbines for power generation. *Appl. Energy* **2016**, *165*, 777–788. [[CrossRef](#)]
43. Park, J.; Jung, H.J.; Lee, S.W.; Park, J. A new building-integrated wind turbine system utilizing the building. *Energies* **2015**, *8*, 11846–11870. [[CrossRef](#)]
44. ANSI/ASHRAE/IES Standard 90.1-2013 *Energy Standard for Buildings Except Low-Rise Residential Buildings*; ASHRAE: Atlanta, GA, USA, 2013.
45. Walters, D.K.; Cokljat, D. A three-equation eddy-viscosity model for Reynolds-averaged Navier–Stokes simulations of transitional flow. *J. Fluids Eng.* **2008**, *130*, 121401. [[CrossRef](#)]
46. Clarke, J.A.; Johnstone, C.; Kelly, N.; Strachan, P.A. The simulation of photovoltaic-integrated building facades. *Build. Simul.* **1997**, *97*, 189–195.
47. Solar Photovoltaic Specification. Available online: [http://www.tatapowersolar.com/images/module/downloads/Datasheet%20-%20TP300%20\[June2015\].pdf](http://www.tatapowersolar.com/images/module/downloads/Datasheet%20-%20TP300%20[June2015].pdf) (accessed on 11 October 2017).
48. Sullivan, R.; Lee, E.S.; Selkowitz, S.E. A method of optimizing solar control and daylighting performance in commercial office buildings. In Proceedings of the Thermal Performance of the Exterior Envelopes of Buildings V Conference, Clearwater Beach, FL, USA, 7–10 December 1992.
49. Chong, W.T.; Pan, K.C.; Poh, S.C.; Fazlizan, A.; Oon, C.S.; Badarudin, A.; Nik-Ghazali, N. Performance investigation of a power augmented vertical axis wind turbine for urban high-rise application. *Renew. Energy* **2013**, *51*, 388–397. [[CrossRef](#)]
50. Kim, D.K.; Kim, M.K.; Cha, D.K.; Yoon, S.H. Design of drag-type vertical axis miniature wind turbine using arc shaped blade. *KSEF J. Fluid Mach.* **2006**, *9*, 7–12.
51. Poirazis, H. A report of IEA SHC Task 34 ECBCS Annex 43. In *Double Skin Façades: A Literature Review*; Lund University: Lund, Sweden, 2006; (displayed 22 July 2014).
52. Streicher, W.; Heimrath, R.; Hengsberger, H.; Mach, T.; Waldner, R. (2006, November). State of the Art of Double Skin Facades in Europe: The results of WP1 of the BESTFAÇADE Project. In Proceedings of the AIVC 27th Conference, Lyon, France, 20–22 November 2006.
53. Xue, F.; Li, X. A fast assessment method for thermal performance of naturally ventilated double-skin façades during cooling season. *Sol. Energy* **2015**, *114*, 303–313. [[CrossRef](#)]

54. De Gracia, A.; Navarro, L.; Castell, A.; Cabeza, L.F. Energy performance of a ventilated double skin facade with PCM under different climates. *Energy Build.* **2015**, *91*, 37–42. [[CrossRef](#)]
55. Larsen, S.F.; Rengifo, L.; Filippín, C. Double skin glazed façades in sunny Mediterranean climates. *Energy Build.* **2015**, *102*, 18–31. [[CrossRef](#)]
56. Park, J. Development of Wind Turbine System for Building Envelope and Evaluation of Its Energy Potential. Ph.D. Thesis, Korea Advanced Institute of Science & Technology, Daejeon, Korea, 2017. Available online: [http://library.kaist.ac.kr/thesis02/2017/2017D020125129\\_S1.pdf](http://library.kaist.ac.kr/thesis02/2017/2017D020125129_S1.pdf) (accessed on 17 November 2017).
57. Justus, C.G.; Hargraves, W.R.; Yalcin, A. Nationwide assessment of potential output from wind-powered generators. *J. Appl. Meteorol.* **1976**, *15*, 673–678. [[CrossRef](#)]
58. Seguro, J.V.; Lambert, T.W. Modern estimation of the parameters of the Weibull wind speed distribution for wind energy analysis. *J. Wind Eng. Ind. Aerodyn.* **2000**, *85*, 75–84. [[CrossRef](#)]
59. Grant, A.; Johnstone, C.; Kelly, N. Urban wind energy conversion: The potential of ducted turbines. *Renew. Energy* **2008**, *33*, 1157–1163. [[CrossRef](#)]
60. Billinton, R.; Chen, H.; Ghajar, R. A sequential simulation technique for adequacy evaluation of generating systems including wind energy. *IEEE Trans. Energy Convers.* **1996**, *11*, 728–734. [[CrossRef](#)]



© 2017 by the authors. Licensee MDPI, Basel, Switzerland. This article is an open access article distributed under the terms and conditions of the Creative Commons Attribution (CC BY) license (<http://creativecommons.org/licenses/by/4.0/>).